Recurrent Fusion of *TMPRSS2* and ETS Transcription Factor Genes in Prostate Cancer

Scott A. Tomlins,[1] Daniel R. Rhodes,[1,2] Sven Perner,[7,9] Saravana M. Dhanasekaran,[1] Rohit Mehra,[1] Xiao-Wei Sun,[7] Sooryanarayana Varambally,[1,6] Xuhong Cao,[1] Joelle Tchinda,[7] Rainer Kuefer,[10] Charles Lee,[7] James E. Montie,[3,5,6] Rajal B. Shah,[1,3,5,6] Kenneth J. Pienta,[3,4,5,6] Mark A. Rubin,[7,8] Arul M. Chinnaiyan[1,2,3,5,6]*

Recurrent chromosomal rearrangements have not been well characterized in common carcinomas. We used a bioinformatics approach to discover candidate oncogenic chromosomal aberrations on the basis of outlier gene expression. Two ETS transcription factors, *ERG* and *ETV1*, were identified as outliers in prostate cancer. We identified recurrent gene fusions of the 5′ untranslated region of *TMPRSS2* to *ERG* or *ETV1* in prostate cancer tissues with outlier expression. By using fluorescence in situ hybridization, we demonstrated that 23 of 29 prostate cancer samples harbor rearrangements in *ERG* or *ETV1*. Cell line experiments suggest that the androgen-responsive promoter elements of *TMPRSS2* mediate the overexpression of ETS family members in prostate cancer. These results have implications in the development of carcinomas and the molecular diagnosis and treatment of prostate cancer.

A central aim in cancer research is to identify altered genes that play a causal role in cancer development. Many such genes have been identified through the analysis of recurrent chromosomal rearrangements that are characteristic of leukemias, lymphomas, and sarcomas (*1*). These rearrangements are of two general types. In the first, the promoter and/or enhancer elements of one gene are aberrantly juxtaposed to a proto-oncogene, thus causing altered expression of an oncogenic protein. This type of rearrangement is exemplified by the apposition of immunoglobulin (*IG*) and T cell receptor (*TCR*) genes to *MYC*, leading to activation of this oncogene in B and T cell malignancies, respectively (*2*). In the second, the rearrangement fuses two genes, resulting in the production of a fusion protein that may have a new or altered activity. The prototypic example of this translocation is the *BCR-ABL* gene fusion in chronic myelogenous leukemia (CML) (*3*, *4*). Importantly, this finding led to the development of the promising cancer drug imatinib mesylate (Gleevec) (*5*). In contrast to leukemias, epithelial tumors (carcinomas) display many nonspecific but few recurrent chromosomal rearrangements (*6*). This karyotypic complexity is thought to reflect secondary genomic alterations acquired during tumor progression.

We hypothesized that rearrangements and high-level copy number changes that result in marked overexpression of an oncogene should be evident in DNA microarray data but not necessarily by traditional analytical approaches. In the majority of cancer types, heterogeneous patterns of oncogene activation have been observed; thus, traditional analytical methods that search for common activation of genes across a class of cancer samples (e.g., *t* test or signal-to-noise ratio) will fail to find such oncogene expression profiles. Instead, a method that searches for marked overexpression in a subset of cases is needed. Toward this end, we developed a method termed cancer outlier profile analysis (COPA). COPA seeks to accentuate and identify outlier profiles by applying a simple numerical transformation based on the median and median absolute deviation of a gene expression profile (*7*) (fig. S1A).

Cancer outlier profile analysis. We applied COPA to the Oncomine database (*8*), a compendium of 132 gene expression data sets representing 10,486 microarray experiments. COPA correctly identified several outlier profiles for genes in specific cancer types in which a recurrent rearrangement or high-level amplification is known to occur (Table 1 and fig. S1, B and C). We focused our analyses on outlier profiles of known causal cancer genes, as defined by the Cancer Gene Census (*9*), that ranked in the top 10 outlier profiles in an Oncomine data set (Table 1 and table S1), because we felt these genes would be the most likely to participate

Table 1. Cancer outlier profile analysis (COPA). Genes known to undergo causal mutations in cancer that had strong outlier profiles. "X" indicates literature evidence for the acquired pathognomonic translocation. "XX" indicate that samples in the study were characterized for the indicated translocation. "Y" indicates consistent with known amplification. Double asterisks indicate *ERG* and *ETV1* outlier profiles in prostate cancer. A complete listing of genes known to undergo causal mutations ranking in the top 10 of all studies in Oncomine, along with the relevant references, is included as table S1.

Rank	%	Score	Gene	Cancer	Study	Evidence
1	95	20.056	*RUNX1T1*	Leukemia	(*23*)	XX
1	95	15.4462	*PRO1073*	Renal	(*24*)	X
1	90	12.9581	*PBX1*	Leukemia	(*25*)	XX
1	95	10.03795	*ETV1*	Prostate	(*15*)	**
1	90	7.4557	*WHSC1*	Myeloma	(*26*)	X
1	75	5.4071	*ERG*	Prostate	(*27*)	**
1	75	4.3628	*ERG*	Prostate	(*28*)	**
1	75	4.3425	*CCND1*	Myeloma	(*29*)	X
1	75	3.4414	*ERG*	Prostate	(*15*)	**
1	75	3.3875	*ERG*	Prostate	(*30*)	**
3	95	13.3478	*FGFR3*	Myeloma	(*29*)	X
4	75	2.5728	*ERBB2*	Breast	(*31*)	Y
6	90	6.6079	*ERBB2*	Breast	(*32*)	Y
9	95	17.1698	*ETV1*	Prostate	(*16*)	**
9	90	6.60865	*SSX1*	Sarcoma	(*33*)	X
9	75	2.2218	*ERG*	Prostate	(*34*)	**

[1]Department of Pathology, [2]Bioinformatics Program, [3]Department of Urology, [4]Department of Internal Medicine, [5]Michigan Urology Center, [6]Comprehensive Cancer Center, University of Michigan Medical School, 1301 Catherine Street, Ann Arbor, MI 48109–0602, USA. [7]Department of Pathology, Brigham and Women's Hospital, [8]Dana-Farber Cancer Institute, [9]Department of Pathology, Harvard Medical School, Boston, MA 02115, USA. [10]Department of Urology, Faculty of Medicine, University of Ulm, Ulm 89075, Germany.

*To whom correspondence should be addressed. E-mail: arul@umich.edu

in uncharacterized alterations. The general COPA methodology can be applied to any expression data (*10*).

Outlier profiles for *ERG* and *ETV1* in prostate cancer. In several independent data sets, COPA identified strong outlier profiles in prostate cancer for *ERG* (21q22.3) and *ETV1* (7p21.2) (Table 1), two genes that encode ETS family transcription factors and are involved in oncogenic translocations in Ewing's sarcoma and myeloid leukemias (*11*, *12*). In total, COPA ranked *ERG* or *ETV1* within the top 10 outlier genes in six independent prostate cancer profiling studies.

Fusion of the 5′ activation domain of the Ewing sarcoma breakpoint region 1 (*EWSBR1*) gene to the highly conserved 3′ DNA binding domain of an ETS family member, such as *ERG* [t(21;22)] or *ETV1* [t(7;22)], is characteristic of Ewing's sarcoma (*11*, *13*, *14*). Because translocations involving ETS family members are functionally redundant in oncogenic transformation, only one type of translocation is typically observed in each case of Ewing's sarcoma. We hypothesized that, if *ERG* and *ETV1* are similarly involved in the development of prostate cancer, their outlier profiles should be mutually exclusive—that is, each tumor should overexpress only one of the two genes.

Thus, we examined the joint expression profiles of *ERG* and *ETV1* across several prostate cancer data sets and found that they invariably showed mutually exclusive outlier profiles, consistent with our hypothesis. Exclusive outlier expression of *ERG* and *ETV1* was identified in two large-scale transcriptome studies (*15*, *16*), which profiled grossly dissected prostate tissues with the use of different microarray platforms (Fig. 1). Similar results were obtained in prostate tissue samples obtained by laser capture microdissection (LCM) (fig. S2A). In addition to exclusive outlier expression of either *ERG* or *ETV1* in epithelial cells from prostate cancer or metastatic prostate cancer, *ETV1* and *ERG* were not overexpressed in the precursor lesion prostatic intraepithelial neoplasia (PIN) or adjacent benign epithelia (fig. S2A). The observed exclusive outlier pattern is consistent with other translocations where an activating gene can fuse with multiple partners, such as the fusion of the immunoglobulin heavy chain promoter to *CCND1* or *FGFR3*, t(11,14) or t(4,14), respectively, in specific subsets of multiple myeloma (*17*) (fig. S2B).

Recurrent gene fusion of *TMPRSS2* to *ERG* or *ETV1* in prostate cancer. To determine the mechanism responsible for *ERG* and *ETV1* overexpression, we identified prostate cancer cell lines and clinical specimens that overexpressed *ERG* or *ETV1* by using quantitative polymerase chain reaction (QPCR) (Fig. 2A). The LNCaP prostate cancer cell line and two specimens obtained from a patient with hormone-refractory metastatic disease (MET26-RP, residual primary carcinoma in the prostate, and MET26-LN, a lymph node metastasis) overexpressed *ETV1*. A lymph node metastasis from a second patient (MET-28LN) and two prostate cancer cell lines, VCaP and DuCaP, overexpressed *ERG*. We did not find consistent amplification of *ERG* or *ETV1* in samples with respective transcript overexpression, so we considered the possibility of DNA rearrangements. We measured the expression of *ETV1* exons by exon-walking QPCR in samples that displayed *ETV1* overexpression. We used five primer pairs spanning *ETV1* exons 2 through 7 and found that although LNCaP cells showed essentially uniform overexpression of all measured *ETV1* exons, both MET26 specimens showed >90% reduction in the expression of *ETV1* exons 2 and 3 compared with exons 4 to 7 (Fig. 2B).

To characterize the complete 5′ *ETV1* transcript, we performed 5′ RNA ligase-mediated rapid amplification of cDNA ends (RLM-

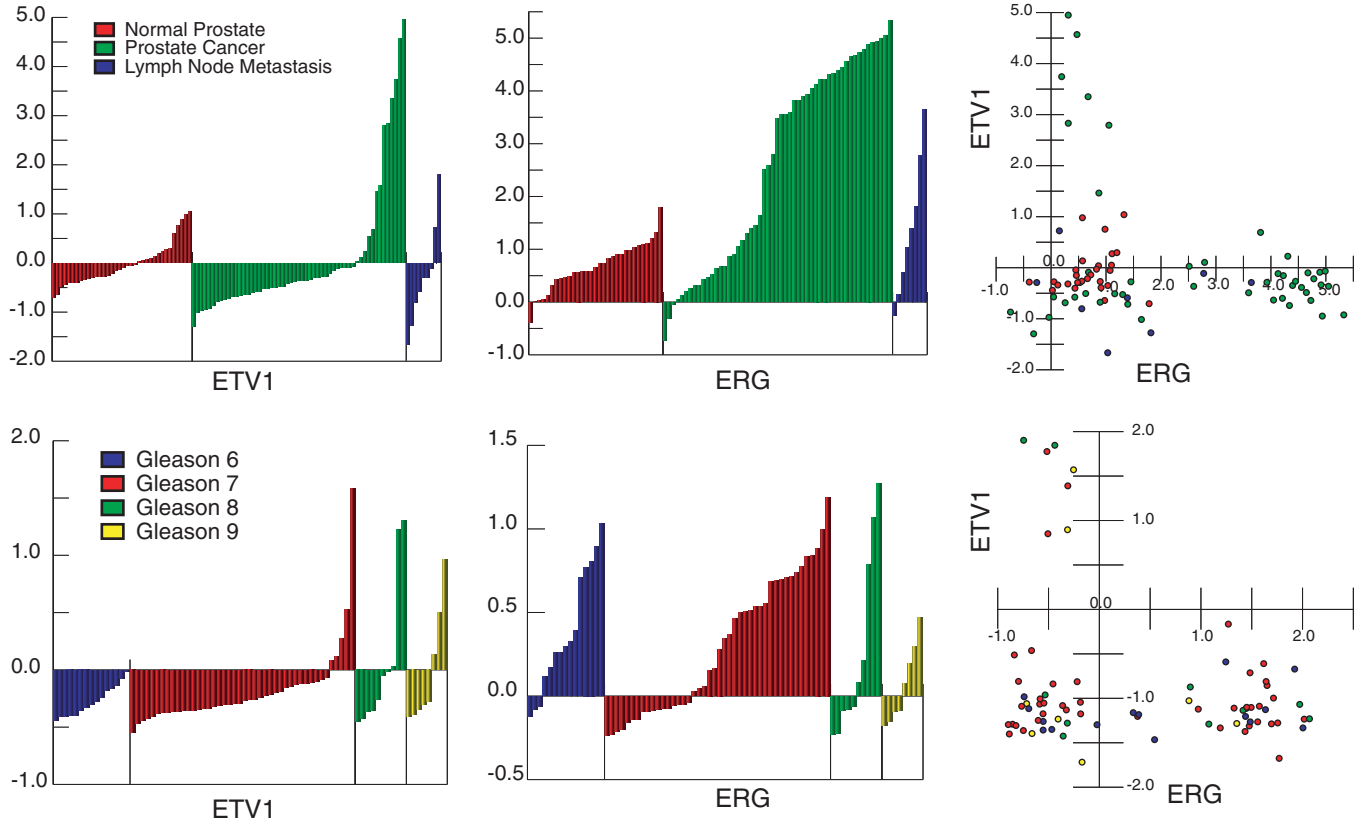

Fig. 1. COPA of microarray data revealed *ETV1* and *ERG* as outlier genes across multiple prostate cancer gene expression data sets. *ETV1* and *ERG* expression (normalized expression units) are shown from all profiled samples in two-large scale gene expression studies [top data set from (*15*) and bottom data set from (*16*)]. Visualization tools incorporated in Oncomine (*10*) were used to generate graphical displays. Sample classes are indicated according to the color scale. In the data set from (*16*), prostate cancer samples were classified on the basis of Gleason grade. Scatter plots of *ERG* and *ETV1* expression across all of the profiled samples are shown (**right**).

RACE) on LNCaP cells and MET26-LN. In addition, we also performed RLM-RACE to obtain the complete 5′ transcript of *ERG* in MET28-LN. Sequencing of the cloned products revealed fusions of the prostate-specific gene *TMPRSS2* (*18*) (21q22.2) with *ETV1* in MET26-LN and with *ERG* in MET28-LN (Fig. 2C). In MET26-LN, two RLM-RACE PCR products were identified. The first product, *TMPRSS2:ETV1a*, resulted in a fusion of the complete exon 1 of *TMPRSS2* with the beginning of exon 4 of *ETV1* (Fig. 2C). The second product, *TMPRSS2:ETV1b*, resulted in a fusion of exons 1 and 2 of *TMPRSS2* with the beginning of exon 4 of *ETV1* (fig. S3). Both products are consistent with the exon-walking QPCR described above, where MET26-LN showed loss of overexpression in exons 2 and 3. In MET28-LN, a single RLM-RACE PCR product was identified, and sequencing revealed a fusion of the complete exon 1 of *TMPRSS2* with the beginning of exon 4 of *ERG* (*TMPRSS2:ERGa*) (Fig. 2C).

Validation of *TMPRSS2:ERG* and *TMPRSS2:ETV1* gene fusions in prostate cancer. On the basis of these results, we designed QPCR primer pairs with forward primers in *TMPRSS2* and reverse primers in exon 4 of *ERG* or *ETV1*. We performed SYBR Green (Molecular Probes, Eugene, OR) QPCR with the use of both primer pairs across a panel of samples from 42 cases of clinically localized prostate cancer and metastatic prostate cancer and depict representative results (Fig. 2, D and E). These 42 cases were selected on the basis of previous cDNA microarray or QPCR results indicating overexpression of *ERG* or *ETV1*. We were limited to samples with remaining material, and thus this cohort does not represent a random sampling. In addition to QPCR, we also performed standard reverse transcription PCR (RT-PCR) with the same primers used for QPCR, or with a different forward primer in *TMPRSS2* and reverse primers in exon 6 of *ERG* and exon 7 of *ETV1* on a subset of the samples with or without fusions as determined by using QPCR (fig. S4, A and B). Electrophoresis of QPCR products and sequencing of cloned RT-PCR products from MET-26RP and MET-26LN revealed the presence of both *TMPRSS2:ETV1a* and *TMPRSS2:ETV1b*. The molecular evidence for *TMPRSS2:ERG* and *TMPRSS2:ETV1* fusions in cases and cell lines overexpressing the respective ETS family member are summarized (fig. S5). From QPCR melt curve analysis and gel electrophoresis of QPCR and RT-PCR products, PCA4 produced a larger amplicon than *TMPRSS2:ERGa*. Subsequent RLM-RACE analysis and sequencing of the RT-PCR product confirmed a fusion of the complete exon 1 of *TMPRSS2* with the beginning of exon 2 of *ERG* (*TMPRSS2:ERGb*) (fig. S3). Evidence for the *TMPRSS2:ERG* and *TMPRSS2:ETV1* fusions were only found in cases that overexpressed *ERG* or *ETV1*, respectively, by QPCR or DNA microarray. These results are also in agreement with the exclusive expression observed in our outlier analysis.

Genomic confirmation of *TMPRSS2:ETV1* translocation and *ERG* rearrangement. We used interphase fluorescence in situ hybridization (FISH) to validate the rearrangements at the chromosomal level on formalin-fixed paraffin-embedded (FFPE) specimens from the two cases initially used for RLM-RACE, MET26 and MET28 (Fig. 3). With the use of probes for *TMPRSS2* and *ETV1*, normal peripheral lymphocytes (NPLs) demonstrated a pair of red and a pair of green signals (Fig.

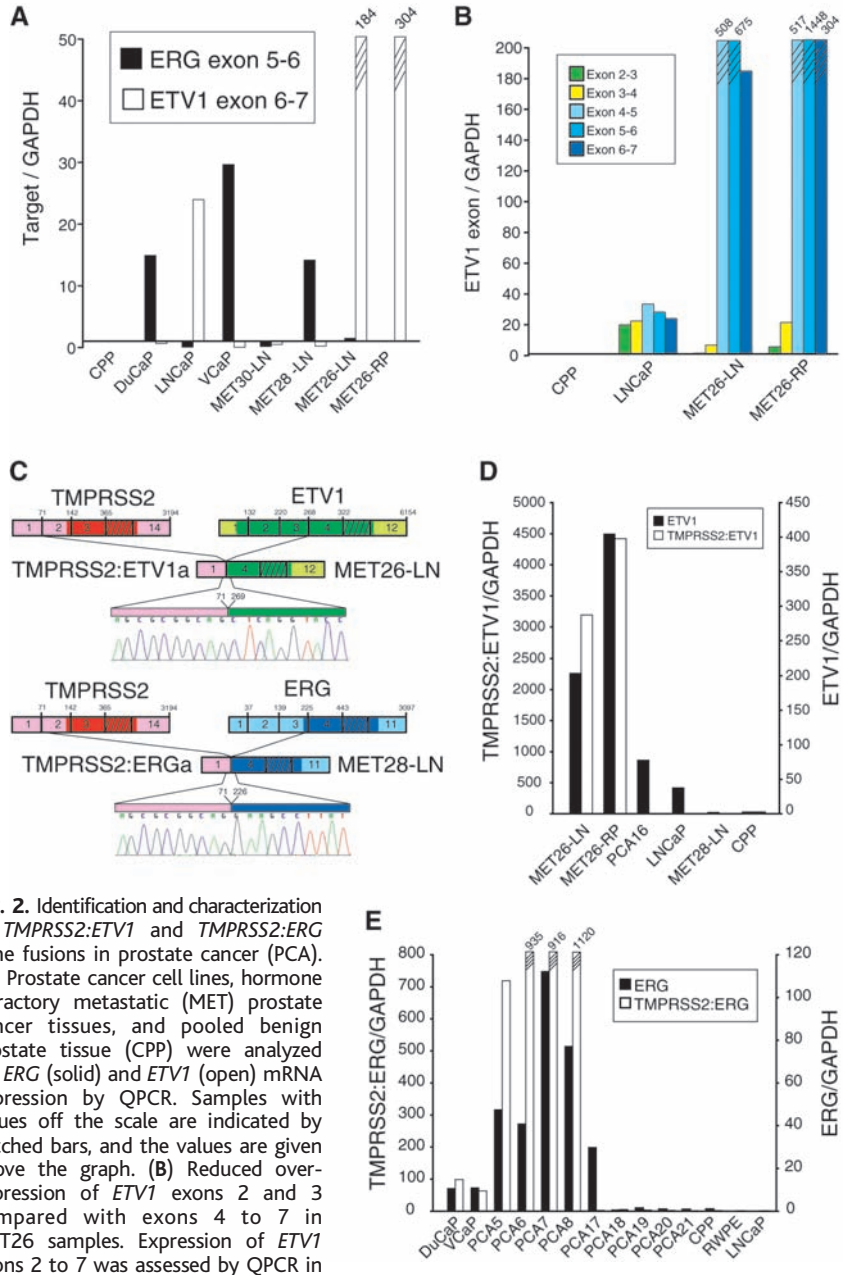

Fig. 2. Identification and characterization of *TMPRSS2:ETV1* and *TMPRSS2:ERG* gene fusions in prostate cancer (PCA). (**A**) Prostate cancer cell lines, hormone refractory metastatic (MET) prostate cancer tissues, and pooled benign prostate tissue (CPP) were analyzed for *ERG* (solid) and *ETV1* (open) mRNA expression by QPCR. Samples with values off the scale are indicated by hatched bars, and the values are given above the graph. (**B**) Reduced overexpression of *ETV1* exons 2 and 3 compared with exons 4 to 7 in MET26 samples. Expression of *ETV1* exons 2 to 7 was assessed by QPCR in LNCaP cells and MET26-LN and MET26-RP samples. (**C**) Schematic of 5′ RLM-RACE revealing fusion of *TMPRSS2* with *ETV1* in MET26-LN and *ERG* in MET28-LN. Structures for the *TMPRSS2*, *ERG*, and *ETV1* genes have their basis in the GenBank reference sequences. The numbers above the exons (indicated by boxes) indicate the last base of each exon. Untranslated regions are shown in corresponding lighter shades. Coding exons not depicted are indicated by hatched boxes. Identified *TMPRSS2* fusions are colored and numbered from the original reference sequences. Line graphs show the position and automated DNA sequencing of the fusion points. (**D**) Validation of *TMPRSS2:ETV1* expression using fusion-specific QPCR in MET26-LN and MET26-RP. Expression of *ETV1* (solid, right axis) and *TMPRSS2:ETV1* (open, left axis) was assessed by QPCR. (**E**) Validation of *TMPRSS2:ERG* expression using fusion-specific QPCR in cell lines and PCA specimens. Expression of *ERG* (solid, right axis) and *TMPRSS2:ERG* (open, left axis) was assessed by QPCR.

3A). However, MET26 showed fusion of one pair of signals, indicative of probe overlap (Fig. 3B) and consistent with the expression of the *TMPRSS2:ETV1*. Because of the proximity of *TMPRSS2* to *ERG* on chromosome 21, ~3 megabases (fig. S6A), we used probes spanning the 5′ and 3′ regions of the *ERG* locus to assay for gene rearrangements. By using these probes, we observed a pair of yellow signals in NPLs (Fig. 3C); however, in MET28, one pair of probes split into separate green and red signals, indicative of a rearrangement at the *ERG* locus (Fig. 3D) and consistent with the expression of *TMPRSS2:ERG*. We next performed both individual FISH analyses described above on serial tissue microarrays containing cores from 13 cases of localized prostate cancer and 16 cases of metastatic prostate cancer (Fig. 3E). Of 29 cases, 23 (79.3%) showed evidence of *TMPRSS2:ETV1* fusion (7 cases) or *ERG* rearrangement (16 cases).

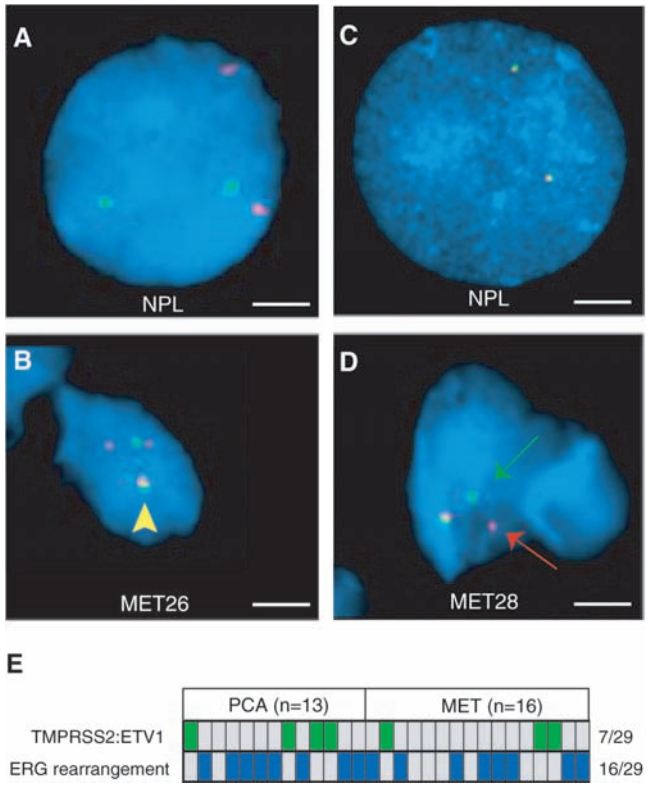

Fig. 3. Interphase FISH on FFPE tissue sections confirms *TMPRSS2:ETV1* gene fusion and *ERG* gene rearrangement. (**A** and **B**) NPLs showed two *ETV1* (red) and two *TMPRSS2* (green) signals, whereas MET26 showed fusion of the signals as indicated by the yellow signal (yellow arrowhead). (**C** and **D**) For detection of *ERG* gene rearrangements, we used a split-signal approach, with two probes spanning the *ERG* locus. NPLs showed two yellow signals, indicating overlap of the 5′ (green signal) and 3′ (red signal) regions of *ERG*, whereas MET28 shows a rearrangement of *ERG* as indicated by the split signal of the 5′ and 3′ probes (red and green arrows). Scale bars for all images are 2.5 μm. (**E**) Matrix representation of FISH results using the same probes as (A) to (D) on an independent tissue microarray containing cores from clinically localized (PCA) and metastatic (MET) prostate cancer. Cores positive for *TMPRSS2:ETV1* probe fusion or split-signal *ERG* probes are indicated by colored cells. All negative findings are indicated by gray cells. The number of positive cases for each feature is indicated to the right of the matrix.

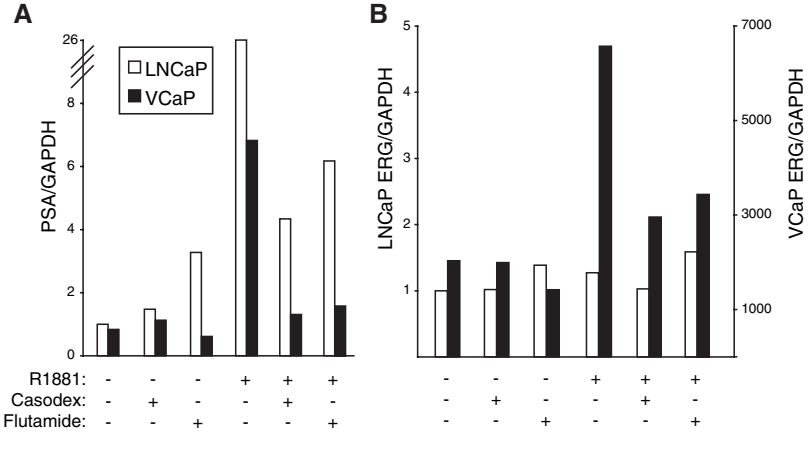

Fig. 4. Androgen regulation of *ERG* in VCaP prostate cancer cells carrying the *TMPRSS2:ERG* fusion. (**A**) *PSA* expression relative to *GAPDH* in androgen-sensitive LNCaP (open) and VCaP (solid) cells was assessed by QPCR. (**B**) *ERG* (exon 5 to 6) expression relative to *GAPDH* in LNCaP (open, left axis) and VCaP (solid, right axis) cells. Cell lines were incubated with vehicle or 10 μM of the androgen receptor antagonists bicalutamide or flutamide for 2 hours before treatment for 24 hours with 0.5 nM of the synthetic androgen R1881 or vehicle as indicated. Relative *PSA* or *ERG* for each sample was normalized to the amount in the LNCaP control.

As additional confirmation of the *ERG* rearrangement, we performed FISH on metaphase spreads of VCaP cells, which express the *TMPRSS2:ERGa* transcript. This assay revealed co-localization of 5′ *TMPRSS2* and 3′ *ERG* probes with splitting of the 5′ and 3′ *ERG* signals, supporting the molecular results (fig. S6). In addition, Southern blotting using a probe in the intron between exons 1 and 2 of *TMPRSS2* revealed a unique band in VCaP cells, consistent with a rearrangement at this locus (fig. S7).

Fusion of *TMPRSS2* and *ERG* results in androgen regulation of *ERG*. *TMPRSS2* is expressed in normal and neoplastic prostate tissue and is strongly induced by androgen in androgen-sensitive prostate cell lines (*18–20*). To investigate whether the *TMPRSS2:ERG* fusion results in the androgen regulation of *ERG*, we assessed the expression of *ERG* by QPCR in androgen-treated VCaP cells, which express *TMPRSS2:ERGa*, and LNCaP cells, which do not express a fusion transcript. Both VCaP and LNCaP respond to androgen stimulation with increased expression of *PSA*, which is expressed at a similar amount in both cells and is sensitive to the androgen receptor antagonists bicalutamide and flutamide (Fig. 4A). However, in addition to expressing ~2000-fold more *ERG* than LnCAP cells, only VCaP cells responded to androgen stimulation with increased *ERG* expression sensitive to bicalutamide and flutamide (Fig. 4B). A similar increase in *ERG* expression upon androgen stimulation was observed in DuCaP cells, which express *TMPRSS2:ERGa*, whereas RWPE, PC3, and PC3 cells expressing the human androgen receptor express low concentrations of *ERG* that are not androgen-responsive (fig. S8). These results suggest that the fusion with *TMPRSS2* may explain the aberrant expression of *ERG* or *ETV1* in specific subsets of prostate cancer.

Conclusions. The existence of recurring gene fusions of *TMPRSS2* to the oncogenic ETS family members *ERG* and *ETV1* may have important implications for understanding prostate cancer tumorigenesis and developing novel diagnostics and targeted therapeutics. Several lines of evidence suggest that these rearrangements occur in the majority of prostate cancer samples and drive ETS family member expression. Across three independent microarray data sets, *ERG* or *ETV1* was markedly overexpressed in 95 of 167 (57%) prostate cancer cases, whereas overexpression was never observed across 54 benign prostate tissue samples. Furthermore, a recent study reported that *ERG* was the most commonly

overexpressed oncogene by QPCR in prostate cancer, with 72.0% of cases overexpressing *ERG* (*21*). By using a combination of assays, we found evidence of fusion with *TMPRSS2* in 20 of 22 (>90%) cases that overexpressed *ERG* or *ETV1*, suggesting that the fusion is the most likely cause for the overexpression. FISH analysis on a set of 29 prostate cancer cases selected independently of any knowledge of *ERG* or *ETV1* expression indicates that 23 of 29 (79%) had *TMPRSS2:ETV1* fusions or *ERG* rearrangement. It is possible that this cohort is not representative of all prostate cancer samples and that this may be an overestimate of the prevalence of *TMPRSS2* fusions with ETS family members, because our split-signal approach can detect additional rearrangements involving *ERG*. However, the reported frequencies of *ERG* or *ETV1* overexpression in prostate cancer with our fusion transcript and FISH results suggest that *TMPRSS2* fusions with *ETV1* or *ERG* occur in the majority of prostate cancer cases. Coupled with the high incidence of prostate cancer [an estimated 232,090 new cases will be diagnosed in the United States in 2005 (*22*)], the *TMPRSS2* fusion with ETS family members is likely to be the most common rearrangement yet identified in human malignancies and the only rearrangement present in the majority of one of the most prevalent carcinomas.

Future efforts will be directed at characterizing the expressed protein products, including the effects of N-terminal truncation of ERG and ETV1, and identifying downstream targets and the functional role of the fusions in prostate cancer development. Importantly, the existence of *TMPRSS2* fusions with ETS family members in prostate cancer suggests that causal gene rearrangements may exist in common epithelial cancers but may be masked by the multiple nonspecific chromosomal rearrangements that occur during tumor progression.

References and Notes

1. J. D. Rowley, *Nat. Rev. Cancer* **1**, 245 (2001).
2. T. H. Rabbitts, *Nature* **372**, 143 (1994).
3. J. D. Rowley, *Nature* **243**, 290 (1973).
4. A. de Klein *et al.*, *Nature* **300**, 765 (1982).
5. M. Deininger, E. Buchdunger, B. J. Druker, *Blood* **105**, 2640 (2005).
6. F. Mitelman, *Mutat. Res.* **462**, 247 (2000).
7. Materials and methods are available as supporting material on *Science* Online.
8. D. R. Rhodes *et al.*, *Neoplasia* **6**, 1 (2004).
9. P. A. Futreal *et al.*, *Nat. Rev. Cancer* **4**, 177 (2004).
10. Detailed results from the application of COPA to Oncomine data sets can be explored at www.oncomine.org.
11. T. Oikawa, T. Yamada, *Gene* **303**, 11 (2003).
12. T. Hsu, M. Trojanowska, D. K. Watson, *J. Cell. Biochem.* **91**, 896 (2004).
13. I. S. Jeon *et al.*, *Oncogene* **10**, 1229 (1995).
14. P. H. Sorensen *et al.*, *Nat. Genet.* **6**, 146 (1994).
15. J. Lapointe *et al.*, *Proc. Natl. Acad. Sci. U.S.A.* **101**, 811 (2004).
16. G. V. Glinsky, A. B. Glinskii, A. J. Stephenson, R. M. Hoffman, W. L. Gerald, *J. Clin. Invest.* **113**, 913 (2004).
17. R. Fonseca *et al.*, *Cancer Res.* **64**, 1546 (2004).
18. B. Lin *et al.*, *Cancer Res.* **59**, 4180 (1999).
19. D. E. Afar *et al.*, *Cancer Res.* **61**, 1686 (2001).
20. E. Jacquinet *et al.*, *Eur. J. Biochem.* **268**, 2687 (2001).
21. G. Petrovics *et al.*, *Oncogene* **24**, 3847 (2005).
22. A. Jemal *et al.*, *CA Cancer J. Clin.* **55**, 10 (2005).
23. P. J. Valk *et al.*, *N. Engl. J. Med.* **350**, 1617 (2004).
24. J. R. Vasselli *et al.*, *Proc. Natl. Acad. Sci. U.S.A.* **100**, 6958 (2003).
25. M. E. Ross *et al.*, *Blood* **102**, 2951 (2003).
26. E. Tian *et al.*, *N. Engl. J. Med.* **349**, 2483 (2003).
27. S. M. Dhanasekaran *et al.*, *FASEB J.* **19**, 243 (2005).
28. J. B. Welsh *et al.*, *Cancer Res.* **61**, 5974 (2001).
29. F. Zhan *et al.*, *Blood* **99**, 1745 (2002).
30. S. M. Dhanasekaran *et al.*, *Nature* **412**, 822 (2001).
31. E. Huang *et al.*, *Lancet* **361**, 1590 (2003).
32. C. Sotiriou *et al.*, *Proc. Natl. Acad. Sci. U.S.A.* **100**, 10393 (2003).
33. T. O. Nielsen *et al.*, *Lancet* **359**, 1301 (2002).
34. Y. P. Yu *et al.*, *J. Clin. Oncol.* **22**, 2790 (2004).

35. We thank D. Roulston and E. Fearon for helpful discussions, D. Robins and K. Burnstein for the PC3+AR cells, and R. Desphande and C. Creighton for technical assistance. Supported by the Early Detection Research Network Biomarker Developmental Lab UO1 CA111275-01 (to A.M.C.); NIH Prostate specialized program of research excellence (SPORE) P50CA69568 (to K.J.P), RO1 CA97063 (to A.M.C.), and R01AG21404 (to M.A.R.); American Cancer Society RSG-02-179-MGO (to A.M.C.); Department of Defense (PC040517 to R.M. and PC020322 to A.M.C.); and the Cancer Center Bioinformatics Core (support grant 5P30 CA46592). D.R.R. is supported by the Cancer Biology Training Program. K.J.P. is an American Cancer Society Clinical Research Professor. A.M.C. is a Pew Biomedical Scholar, and S.A.T. and D.R.R. are Fellows of the Medical Scientist Training Program. Nucleotide sequences for the *TMPRSS2:ETS* fusions have been deposited at GenBank with accession numbers DQ204770 to DQ04773.

Supporting Online Material

www.sciencemag.org/cgi/content/full/310/5748/644/DC1
Materials and Methods
Figs. S1 to S8
Tables S1 and S2

20 July 2005; accepted 22 September 2005
10.1126/science.1117679

REPORTS

Hanbury Brown Twiss Effect for Ultracold Quantum Gases

M. Schellekens,[1] R. Hoppeler,[1] A. Perrin,[1] J. Viana Gomes,[1,2] D. Boiron,[1] A. Aspect,[1] C. I. Westbrook[1]*

We have studied two-body correlations of atoms in an expanding cloud above and below the Bose-Einstein condensation threshold. The observed correlation function for a thermal cloud shows a bunching behavior, whereas the correlation is flat for a coherent sample. These quantum correlations are the atomic analog of the Hanbury Brown Twiss effect. We observed the effect in three dimensions and studied its dependence on cloud size.

Nearly half a century ago, Hanbury Brown and Twiss (HBT) performed a landmark experiment on light from a gaseous discharge (*1*). The experiment demonstrated strong correlations in the intensity fluctuations at two nearby points in space despite the random or chaotic nature of the source. Although the effect was easily understood in the context of classical statistical wave optics, the result was surprising when viewed in terms of the quantum theory. It implied that photons coming from widely separated points in a source such as a star were "bunched." On the other hand, photons in a laser were not bunched (*2*, *3*). The quest to understand the observations stimulated the birth of modern quantum optics (*4*). The HBT effect has since found applications in many other fields from particle physics (*5*) to fluid dynamics (*6*).

Atom or photon bunching can be understood as a two-particle interference effect (*7*). Experimentally, one measures the joint probability for two particles emitted from two separated source points, A and B, to be detected at two detection points, C and D. One must consider the quantum mechanical amplitude for the process $A \rightarrow C$ and $B \rightarrow D$ as well as that for $A \rightarrow D$ and $B \rightarrow C$. If the two processes are indistinguishable, the amplitudes interfere. For bosons, the interference is constructive, resulting in a joint detection probability that is enhanced compared with that of two statistically independent detection events, whereas for fermions the joint probability is lowered. As the detector separation is increased, the phase difference between the two amplitudes grows large enough that an average over all possible source points A and B washes out the interference, and one recovers the sit-

[1]Laboratoire Charles Fabry de l'Institut d'Optique, UMR 8501 du CNRS, Centre Scientifique d'Orsay, Bâtiment 503, 91403 Orsay CEDEX, France. [2]Departimento de Fisica, Universidade do Minho, 4710-057 Braga, Portugal.

*To whom correspondence should be addressed. E-mail: christoph.westbrook@iota.u-psud.fr

Recurrent Fusion of TMPRSS2 and ETS Transcription Factor Genes in Prostate Cancer

Scott A. Tomlins, Daniel R. Rhodes, Sven Perner, Saravana M. Dhanasekaran, Rohit Mehra, Xiao-Wei Sun, Sooryanarayana Varambally, Xuhong Cao, Joelle Tchinda, Rainer Kuefer, Charles Lee, James E. Montie, Rajal B. Shah, Kenneth J. Pienta, Mark A. Rubin, and Arul M. Chinnaiyan

Science, 310 (5748), • DOI: 10.1126/science.1117679